An in silico study on the role of smooth muscle cell migration in neointimal formation after coronary stenting

Tahir, H.; Niculescu, I.; Bona-Casas, C.; Merks, R.M.H.; Hoekstra, A.G.

Citation for published version (APA):
Tahir, H., Niculescu, I., Bona-Casas, C., Merks, R. M. H., & Hoekstra, A. G. (2015). An *in silico* study on the role of smooth muscle cell migration in neointimal formation after coronary stenting. *Journal of the Royal Society Interface*, *12*(108), Article 20150358. https://doi.org/10.1098/rsif.2015.0358

INTERFACE

Research

CrossMark
click for updates

Author for correspondence:
Hannan Tahir
e-mail: h.tahir@cwi.nl

†Present address: Department of Orthopedic Surgery, VU Medical Centre, Amsterdam and Life Sciences Group, Centrum Wiskunde en Informatica, Amsterdam, The Netherlands.
‡Present address: Theoretical Biology and Bioinformatics, Utrecht University, Utrecht, The Netherlands.

THE ROYAL SOCIETY
PUBLISHING

An *in silico* study on the role of smooth muscle cell migration in neointimal formation after coronary stenting

Hannan Tahir[1,†], Ioana Niculescu[1,2,‡], Carles Bona-Casas[1],
Roeland M. H. Merks[2,3] and Alfons G. Hoekstra[1,4]

[1]Computational Science Laboratory, Informatics Institute, University of Amsterdam, Amsterdam, The Netherlands
[2]Life Sciences Group, Centrum Wiskunde and Informatica, Amsterdam, The Netherlands
[3]Mathematical Institute, Leiden University, Leiden, The Netherlands
[4]National Research University ITMO, Saint Petersburg, Russia

RMHM, 0000-0002-6152-687X

Excessive migration and proliferation of smooth muscle cells (SMCs) has been observed as a major factor contributing to the development of in-stent restenosis after coronary stenting. Building upon the results from *in vivo* experiments, we formulated a hypothesis that the speed of the initial tissue re-growth response is determined by the early migration of SMCs from the injured intima. To test this hypothesis, a cellular Potts model of the stented artery is developed where stent struts were deployed at different depths into the tissue. An extreme scenario with a ruptured internal elastic lamina was also considered to study the role of severe injury in tissue re-growth. Based on the outcomes, we hypothesize that a deeper stent deployment results in on average larger fenestrae in the elastic lamina, allowing easier migration of SMCs into the lumen. The data also suggest that growth of the neointimal lesions owing to SMC proliferation is strongly dependent on the initial number of migrated cells, which form an initial condition for the later phase of the vascular repair. This mechanism could explain the *in vivo* observation that the initial rate of neointima formation and injury score are strongly correlated.

1. Introduction

Coronary arteries supply blood to the heart, and the walls of these arteries have three distinct layers: the intima is the innermost layer composed of a single layer of endothelial cells (ECs) supported by a non-cellular, elastic membrane called internal elastic lamina (IEL). The middle layer is called media and it mainly contains smooth muscle cells (SMCs) surrounded by a thin external elastic lamina (EEL). The adventitial layer is the outer layer of the artery wall and generally consists of collagen and elastic tissue. Under pathological conditions, a plaque of fatty deposits builds up and reduces the blood supply to the heart muscles. The closure of the coronary artery owing to the presence of such plaques is known as coronary stenosis. The most common treatment option for such a stenosis is balloon angioplasty followed by stent deployment: a balloon is guided towards the blocked site and inflated in order to reopen the artery. A metallic mesh-like structure, called the stent, is placed to hold the artery in an opened position. In many cases, however, in response to this treatment, the tissue regrows and closes the artery again: this condition is called in-stent restenosis (ISR). In this paper, we develop a computational approach to help understand the cellular mechanisms of ISR.

Balloon angioplasty and stent deployment partially or completely denude the endothelial layer and may stretch, or even rupture the IEL [1–3]. This arterial injury activates platelet aggregation, triggers the migration and proliferation of SMCs and stimulates the production of extracellular matrix (ECM) materials. Together, these responses result in a regrowth of the tissue known as ISR [4]. Although ISR involves an interplay between platelets, monocytes, SMCs, fibroblast, etc., the migration of SMCs through the injured intima and their further

proliferation into the lumen are considered to be the prime culprits in this complex phenomenon [5,6].

The fenestrae in the IEL may act to provide enhanced communication between the vascular ECs and the SMCs [7]. Moreover, the role of IEL fenestrae has also been suggested to play a part in the SMC migration from the medial layer into the intima [8,9]. The morphological changes in the IEL owing to balloon angioplasty and stenting might have an impact on the migration of underlying SMCs and may affect the growth dynamics of ISR. According to Gunn *et al.* [3], neointima (the new tissue layer formed due to the arterial injury) can still develop in the presence of an un-broken IEL, and there seems to be a direct correlation between the IEL stretch, based on the angle between the IEL and the stent strut, and the final neointima in porcine animal experiments [3] as well as with the initial rate of neointima formation [3,10].

Right after vascular injury, SMCs from the medial wall have been observed to migrate through the IEL fenestrae into the lumen where they start to proliferate [9,11]. Under physiological conditions, SMCs tend to remain in a contractile quiescent state (G0 of the cell cycle). However, after the arterial injury, some of these cells change their phenotypes and enter the G1 growth phase [12]. During the G1 phase, an increase in the cell volume along with an increase in the cell viscosity takes place [13]. The cell becomes less adhesive to its neighbours in the later phase of the G1 (G$_{1b}$) cell cycle, provoking cell migration [13]. Fukui *et al.* [13] observed most of the cultured migrating SMCs in the later G1 phase of the cell cycle and this seems to be consistent with other studies related to drugs such as rapamycin or paclitaxel which have been used to block the cell cycle progression. Those studies reported the inhibition of cells migration owing to the presence of drugs [14,15].

Several modelling methodologies (finite-element, cell-based, lattice based) have been adapted in the past to model different aspects of ISR both at tissue and cellular levels [10,16–19]. Cell-based models, including off-lattice, agent-based models (ABMs) or cellular Potts models (CPMs), can simulate the dynamics of the functions occurring at the cellular level in a relatively straightforward way. In earlier work, we have developed ABMs fully coupled with blood flow to simulate the process of ISR [10,16,17] where the ISR final growth response owing to injury and the role of re-endothelialization on ISR have been studied. However, these models do not allow one to incorporate the SMC migration through the IEL layer and instead, a broken IEL layer has always been used to estimate the injury. In comparison with our previous ABMs, CPM permits both the migration through the IEL fenestrae and proliferation of cells at the same time, which makes it a better choice for simulating the initial phases of ISR. Recent developments in the CPM allow one to replicate the stress–strain relationship of tissues, e.g. the vascular wall, by linking cells or subvolumes of the ECM with springs [20] or using hybrids between the CPM and mechanical finite-element models [21]. We developed a CPM of the stented vessel to study the basic mechanisms in the initial phase of the ISR response.

In this paper, we formulate the hypothesis that SMC migration during the early events after vascular injury might be the main cause leading to the development of ISR and that the amount of ISR directly correlates with the amount of early SMC migration. To support this hypothesis, we developed a CPM of stent placement in a pig coronary artery. We use the model to study potential cellular mechanisms during
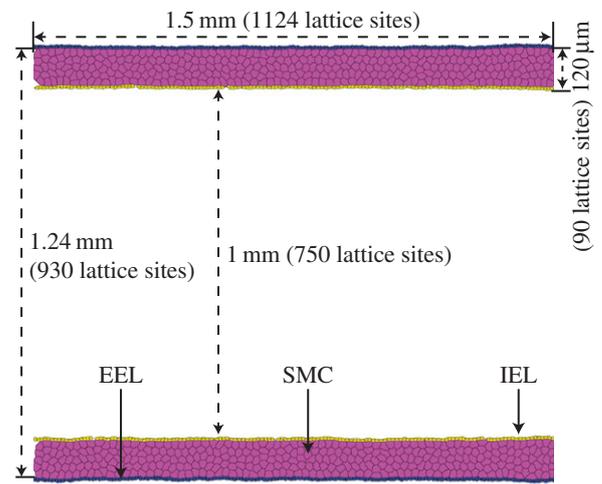
2

Figure 1. A benchmark two-dimensional un-stented vessel composed of contractile SMCs (middle layer, pink) and two laminae. IEL is shown in yellow (top layer) whereas EEL is shown in blue (bottom layer). (Online version in colour.)

the initial phases of ISR. The results and growth trends are qualitatively compared with available *in vivo* data and other published *in silico* models.

2. Material and methods

2.1. Computational model of in-stent restenosis

ISR is a complex pathophysiological response involving an interplay of biochemical and biomechanical effects. As endothelium is usually damaged or dysfunctional during the early days, shear stresses occurring from the blood flow are particularly important during the middle and later phases of ISR progression, where they mitigate ISR growth [22–24]. The effect of flow shear stresses on the growth and tissue morphology of ISR afflicted vessel walls has already been highlighted in our previous studies using coupled ISR models [10,16]. However, the early phases of ISR that we focus on here seem to be mainly dependent on the extent of injury to the vascular wall [3]. Therefore, this study does not include the role of blood flow.

The CPM was introduced by Graner & Glazier [25,26] and has been applied in studies of collective behaviour of cellular structures and of biological development. The CPM describes biological cells as domains on a regular lattice. Each cell has its own identity σ and is represented as a set of lattice sites sharing the same index. Therefore, every lattice site x is a part of one specific cell that has its particular identity $\sigma(x)$. Any lattice site that does not belong to any biological cell type is typically considered as a medium with a cell identification number $\sigma = 0$. Additionally, every cell in the CPM is marked with a label $\tau(\sigma) > 0$ to identify a biological cell type. The classical implementation of the CPM employs a modified metropolis Monte Carlo algorithm to describe amoeboid movement. The dynamics of the cells is described by a globally defined effective Hamiltonian, H, which usually is the sum of terms representing cell adhesion and volume or surface constraints. All the upgrade steps in the CPM are related to the actual biological process of cell expansion and retraction, leading to actual biological kinetics as, for example, shown for cell sorting [25,27]. The CPM is further explained in the electronic supplementary material (text S1).

In this study, a two-dimensional CPM-based ISR model has been developed using the tissue simulation toolkit [28–30]. A two-dimensional vessel (figure 1) with a segment length of 1.5 mm and a lumen width of 1 mm is placed in a rectangular dish (1124 × 1330 lattice sites) corresponding to 1.50 × 1.775 mm where the size of one CPM pixel is 1.3346 μm. The vessel wall thickness is kept at

120 μm based on the typical medial wall thickness observed in porcine histological coronary artery sections [3]. Currently, the vessel wall is solely composed of five layers of SMCs, bounded between two thin elastic layers: IEL and EEL. To achieve this, both elastic lamina layers (IEL and EEL) were first created, and then the SMCs with an average surface area of 445 μm² (≈24 μm in diameter) were seeded to fill the empty space between both laminae.

The medium properties and the energy between the elastic laminae (IEL and EEL) and medium are kept constant throughout the simulations. The magnitude of adhesion between the SMCs and the ECM has been observed to influence the SMC motility [31] and in physiological conditions, the quiescent SMCs (contractile) strongly adhere to the ECM and remain stationary [32]. However, under pathological conditions, the medial SMCs change their phenotype from a contractile (non-proliferative) to a synthetic (proliferative) phenotype [4]. Synthetic SMCs adhere less to the ECM, and they migrate by creating or breaking dynamic attachments with the ECM [33,34]. A similar strategy has been incorporated in the current model by differentiating between these two SMC phenotypic properties where high adhesion energy between cell-type pairs of SMCs and ECM components (IEL and EEL) is selected for contractile SMCs (prior to stenting), whereas a low adhesion energy has been imposed between cell type pairs of SMCs and ECM components post-stenting (synthetic phenotype). A full list of parameters used in the current model is tabulated in table 1. These parameters were selected from another study [35] where a single strut was deployed into a small portion of the artery and a detailed parameter analysis was performed (see electronic supplementary material, text S2, for more details).

2.2. Elastic laminae

We used CPM cells to describe ECM units (IEL and EEL). The monolayers of elastic laminae, both IEL and EEL, are each represented by their own cell type (value of $\tau(\sigma)$) in the model. The lamina 'cells' are assumed to adhere strongly to one another, such that they form a unified membrane; a list of all interaction energies is given in table 1. To maintain mono-layered laminae, every 'cell' in the lamina is connected to the neighbours on either side (right and left) of the same cell type via Hookean springs of resting length $L_T(k)$ connecting the centres of mass. To this end, each link contributes an additional energy bias $H_{elastic}$ in the Hamiltonian [20]

$$H_{elastic} = \sum_{k=link} \lambda_{elastic}(k) \times (l(k) - L_T(k))^2, \quad (2.1)$$

where k is a link, $l(k)$ is the current length of the link, $L_T(k)$ is the specified target length of the link. The term $\lambda_{elastic}(k)$ represents an elasticity parameter, resulting in a stiffer link with a higher $\lambda_{elastic}(k)$ value. The link length $l(k)$ is estimated by calculating the absolute distance between the centres of mass of two cells connected to each other by a link. Rupture of the IEL is permitted by removing IEL links based on the link length. If the length of any IEL link exceeds twice its target link length, we remove that specific link. The first and the last lamina cells on the horizontal boundaries are fixed to the lattice in order to hold the vessel in place during stent deployment.

To generate fenestrae in the IEL, in a set of randomly selected links, we increased the target length ($L_T = 5$ pixels (6.67 μm)) to $L_{TF} = L_T + $ fenestrae_size, with L_{TF} the fenestra size. The gap density is given by the fraction of links to which the enlarged target L_{TF} is assigned. The size of the IEL fenestrae may affect the migration of SMCs from the media into the lumen; therefore, a careful selection of the gap size in the *in silico* model is crucial. We used an average IEL fenestration diameter of 2 pixels (2.669 μm), based on the findings of Kwon *et al.* [36] in the porcine coronary arteries. To observe the effect of this parameter on ISR dynamics, we also varied the fenestration size between 2 and 7 pixels (2.669–9.34 μm). The results from these fenestrae size

Table 1. Simulation parameters.

parameter	value
effective simulation temperature T	25
initial number of quiescent SMCs	700
number of IEL cells	376
number of EEL cells	322
SMC stiffness λ_{SMC}	50
elasticity parameter of elastic laminae $\lambda_{laminae}$ (IEL and EEL)	50
adhesion energy between synthetic SMC (sSMC – sSMC)	70
adhesion energy between quiescent SMC (qSMC – qSMC)	30
adhesion energy between IEL	20
adhesion energy between EEL	5
surface tension between synthetic SMC and IEL	−5
surface tension between synthetic SMC and EEL	12.5
surface tension between synthetic SMC and medium	15
surface tension between quiescent SMC and IEL	75
surface tension between quiescent SMC and EEL	42.5
surface tension between quiescent SMC and medium	45
surface tension between IEL and medium	40
surface tension between EEL and medium	27.5
Monte Carlo step at which quiescent SMCs become synthetic	20 000
Monte Carlo steps in which vessel is initialized and stent is deployed	20 000
total simulation time in Monte Carlo steps	100 000
SMC growth rate during cell cycle r	27.8 μm² h⁻¹

analyses are discussed in the electronic supplementary material (text S2) and shown in electronic supplementary material, figure S2. In addition to the average fenestration size, the mean density of the IEL (the number of holes appearing in a specified area) may also affect the total number of migrated SMCs. In this study, 5.89 gaps per 100 μm is chosen as a gap density based on the highest average rate of appearance reported in [37]. We also evaluated the effects of a lower gap density for IEL (1.5 gaps per 100 μm) on ISR growth and results are discussed and shown in the electronic supplementary material (text S2 and figure S2). The above-mentioned parameters (fenestration size and gap density) are applied in an equilibrium state (pre-stenting), but the stretching of the vessel wall in response to stent deployment affects the equilibrium distance between the IEL cells and hence disturbs the fenestration size, especially near the stent struts where stretch is usually more prominent. This causes an increase in the fenestration size, leaving behind enlarged holes presenting an easy way out for the SMCs to scroll and migrate through the IEL. Naturally, medial and adventitial layers surround the EEL; however, we do not take into account the presence of adventitia and the role of fenestrations in the EEL layer. Addition of EEL fenestrations without the adventitial layer will make it impossible for the SMCs to stop migrating and proliferating outside the EEL area, which is unrealistic. Therefore, we do not consider any fenestrations in the EEL layer.
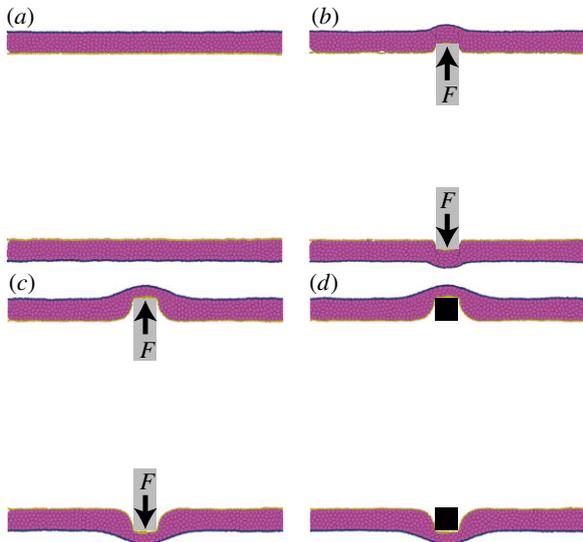
Figure 2. Stent deployment procedure. (a) Un-stented vessel. (b) A force field is initialized at the locations where stent struts will be deployed and this causes the vessel to deform outwards from those locations. (c) Force field is kept switched on until the desired deployment depth is reached. (d) Stent struts are placed inside the vessel and the force field is switched off. (Online version in colour.)

2.3. Stent deployment

The stent struts are deployed in the centre of the vessel section by pushing two square stent struts into the vessel walls. Stent struts are represented by a special cell type impenetrable for the biological cells (i.e. if a cell attempts to copy into the stent, the update is rejected). The stent material is non-adhesive, to which end a high adhesion energy is assigned to the struts.

Smooth muscle cells retain contractile properties until the final deployment depth is achieved. The cross-sectional thickness of the struts is kept constant at 90 μm. The deployment process is modelled by perceiving ΔH (change in the Hamiltonian) as a force field, $F \propto \nabla H$. The force was gradually applied on the tissue perpendicular to the horizontal axis until it reaches a specified deployment depth, after which the stent is introduced and the force is released. The width of the force field is set equivalent to the thickness of the strut and is effective on all the cells at the locations where struts will be deployed (figure 2).

The process of the force field is implemented by biasing the ΔH of all the index change attempts. If an index change attempt is in the direction opposing the deployment direction, a positive value of F is added to the ΔH to discourage the copy attempt; however, if the copy attempt is in a similar direction as the applied force, this is encouraged by subtracting F from ΔH. No restrictions are applied to the index change attempts in the direction perpendicular to the direction of deployment. To achieve a radial expansion in the vessel during stenting, parallel force fields in opposite directions from inside of the vessel are applied to both struts (figure 2b,c). This rule can be stated as

$$\Delta H = \left\{ \begin{array}{ll} \Delta H + \text{sgn}(y_p - y) \times F, & \text{lattice site } x \in \text{force field} \\ \Delta H, & \text{otherwise} \end{array} \right\},$$
(2.2)

for the lower strut, and

$$\Delta H = \left\{ \begin{array}{ll} \Delta H + \text{sgn}(y - y_p) \times F, & \text{lattice site } x \in \text{force field} \\ \Delta H, & \text{otherwise} \end{array} \right\},$$
(2.3)

for the upper strut. Here, sgn is the sign function, y_p is the y-coordinate of the lattice which tries to copy itself in the lattice with a y-coordinate 'y' and F is the applied force. The magnitude

and the duration of the applied force is kept constant for all the simulations presented in this study.

2.4. Smooth muscle cell migration and proliferation

In this study, the time unit is determined by relating the cell cycle progression with the average cell cycle duration of porcine SMCs. A typical cell cycle length of aortic porcine SMCs is 32 h [38], and based on this, an SMC doubles its volume and finally divides into two cells (parent and daughter) every 32 h. Taking that into consideration, we have adjusted the pure doubling speed of the cell (32 h) to 3776 Monte Carlo steps (MCS), resulting in 118 MCS equal to 1 h of real time.

In our model, all SMCs change their phenotype from contractile to synthetic immediately after stent deployment. These SMCs are then allowed to proliferate according to a set of rules.

Cell proliferation is controlled via a cell-cycle rule where a cell initially increases its area until it reaches a prescribed area. It then divides along the short axis into two equal-sized cells (parent and daughter). The transition from contractile to synthetic does not affect the volume of the cell immediately. If the synthetic cell is allowed to grow, the cell volume increases at a fixed rate.

Based on observations of cultured cell colonies of epithelial cells, where cells in the middle of the colonies were identified as quiescent [39–41], we have developed a contact inhibition rule where, if any SMC is completely surrounded by the neighbouring cells and has no contact with the medium, then that specific cell is assumed as contact inhibited. This rule has already been used in our other multiscale ISR models [10,16,17,42].

A checkpoint-oriented cell cycle model has then been used, where the state (G0, G1, G2) of cell is switched based on the contact inhibition rule. If any synthetic SMC is not contact inhibited, the cell enters into the G1 phase where the target area of cell is gradually increased for 16 h until it reaches a critical (doubling) surface area. After this point, the cell enters the G2 state where it just stays for another 16 h before it divides into two cells. The contact inhibition rule is continuously applied throughout the cell cycle to check if the cell remains in contact with the medium. If somehow the cell is no longer attached to the medium during the cell cycle evolution, it is put back to the G0 state while maintaining its current cell area. After division, target volumes for the parent and daughter cells are set to half of the target volume of the mitotic cell just prior to cell division. The parent cell keeps the properties of the actual mitotic cell, whereas the daughter cell is assigned with a new cell index.

Because SMCs are tightly packed within the IEL and EEL, the only possible gaps the SMCs can find to be in contact with the medium are those that exist in the pores of the IEL layer. The SMCs adjacent to such gaps are allowed to leave the G0 state and, if the IEL gaps are wide enough, they can also migrate through them and appear into the lumen where they can continue to proliferate. In real vessels, old ECM degradation, cell detachment, migration and deposition of new ECM are all involved in the process of cell migration. We do not include the role of ECM degradation and deposition in SMC migration. Moreover, the term SMC migration used in this study includes those cells which were pushed out through the IEL owing to SMC proliferation inside the vessel.

2.5. Injury scores

Stent deployment stretches the IEL, widening the fenestrae or breaking it. Based on the condition of the IEL layer, Gunn *et al.* [3] identified three 'injury scores', injury scores 1, 2 and 3. In injury score 1, the IEL remains intact and the angle between the IEL and the base of the strut falls below 45°. For injury score 2, the angle exceeds 45°. For injury score 3, the IEL layer breaks.
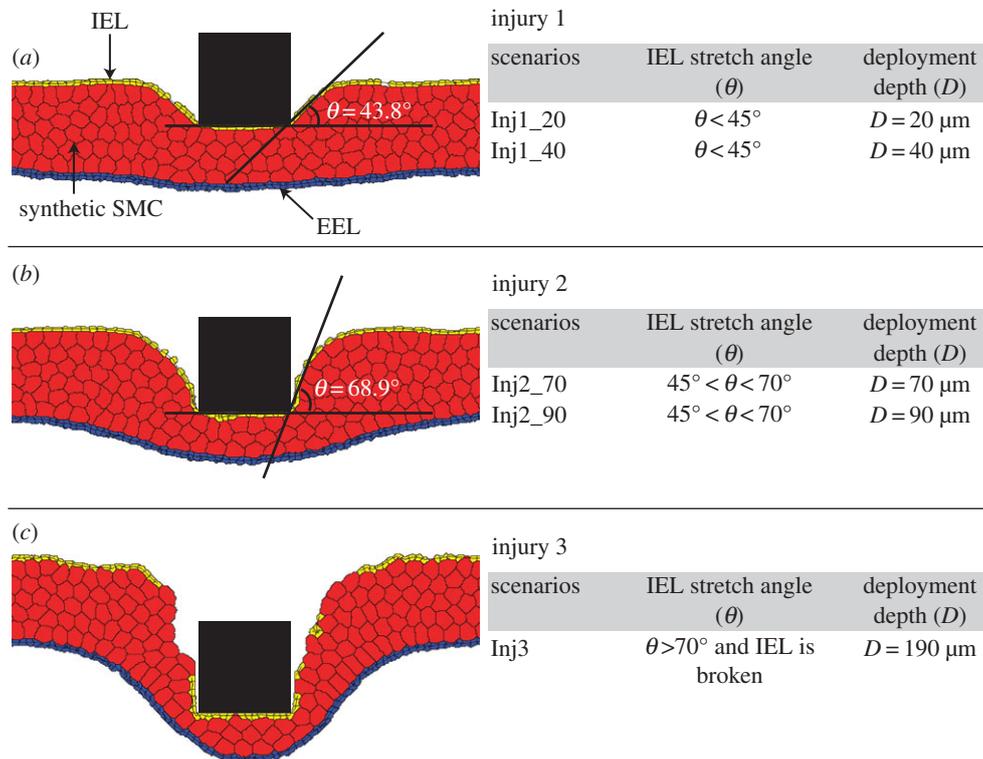
Figure 3. Injury score and angle of IEL stretch. (*a*) Injury score 1 where the angle is below 45°, (*b*) injury score 2 where IEL angle is above 45° and (*c*) injury score 3 where IEL ruptures. The large cells (in red) represent synthetic SMCs, whereas top (yellow) and bottom (blue) linings represent IEL and EEL layers, respectively. (Online version in colour.)

Based on Gunn's injury scores, the injuries are identified in our model by measuring the angle between the IEL and the base of the stent strut (figure 3). Five simulation scenarios are designed in which we deploy struts at increasing depths into the tissue (figure 3). For injury score 1, we test two scenarios: Inj1_20 and Inj1_40 in which struts were deployed at 20 and 40 μm. Similarly, we test two scenarios for injury score 2: Inj2_70 and Inj2_90, where stent deployment depths were 70 and 90 μm. Injury score 3 (Inj3) occurs if the IEL breaks. After breaking, the IEL retracts until it reaches an equilibrium state with 0% strain (figure 3*c*). Apart from injury induced by the stent, balloon angioplasty [43] can trigger neointima formation. We therefore set up an additional scenario (Inj_BA) in which only the complete endothelium was removed, inducing a phenotypic change of the SMCs from contractile to synthetic. This scenario represents a un-stented vessel after balloon angioplasty alone.

3. Results

To characterize how injury owing to stenting or balloon angioplasty affects cell migration, we counted the number of migrated SMCs through the enlarged IEL holes for each scenario. Figure 4 shows a snapshot of the cells migrating through the IEL layer using the scenario Inj2_90. The black arrows indicate those cells that have entered into G1 and started migration. The number of migrated SMCs that crossed the IEL barrier within the first two weeks after stenting were counted for each scenario. The decision to count a cell as migrated is based on a careful visual inspection from the images, which were generated every hour for each simulation. Visual inspection allows us to distinguish migration from proliferation of neointimal cells: we counted only cells which migrated through the IEL for the first time, thus excluding cells appearing in the lumen owing to proliferation of migrated cells. Figure 5 shows the migration of SMCs for all injury scenarios. In the Inj3 scenario, the
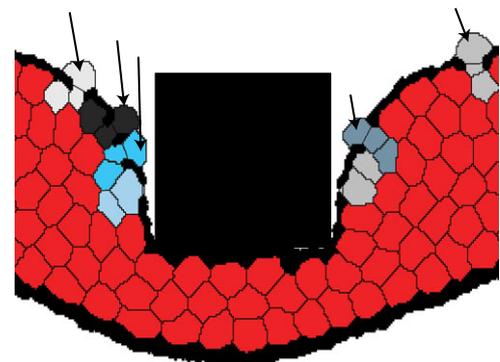

Figure 4. A small portion of the vessel near the stent strut showing the migration of SMCs through the IEL fenestrae. Black arrows show those specific SMCs which have started migrating through the IEL gaps. The majority of cells (in red) are the synthetic SMCs, whereas the other (non-red) cells show the SMCs which initially entered into the cell cycle but could not migrate or get through the IEL layer into the lumen and finally proliferated inside the vessel wall. The snapshot is taken at 24 h post-stenting and the strut deployment depth is 90 μm (Inj2_90). The IEL and EEL cells are now coloured black. (Online version in colour.)

broken IEL layer complicates the cell migration counts: the SMCs which are no longer contact inhibited by the IEL layer are also counted as migrated SMCs. These exposed cells can immediately enter into the cell cycle and give rise to neointima.

Every scenario is simulated 10 times. Results are expressed as means ± s.d. The averaged results of the number of migrated SMCs through the IEL as a function of time are shown in figure 5. It is clear from figure 5 that the migration of SMCs increases with an increase of the vascular injury. However, no differences between the Inj_BA and the two Inj1 scenarios can be observed. Additionally, the SMC migration among all injury groups appears to stop approximately within the first
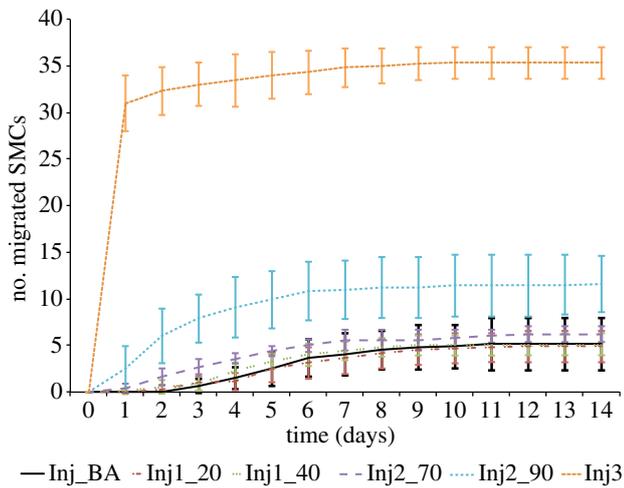
Figure 5. Number of SMCs migrated as a function of time for all the injury scenarios. (Note that the inj_BA curve is hardly visible and overlaps with the inj1_20 curve.) (Online version in colour.)

week after injury. This is due to the fact that once an SMC migrates through the pore of the IEL, it starts to proliferate at that location, thus blocking the passage for other SMCs through that specific pore. Figure 5 also highlights a significant increase in the number of migrated SMCs in the Inj3 scenario, where the IEL ruptures, when compared with the other injury scores.

Figure 6 shows the progression of neointimal development owing to SMC proliferation at 7, 14 and 21 days post-stenting. To further characterize the formation of neointimal tissue in our model, separate colours were applied to the initial synthetic cells as soon as they started to divide for the first time, such that each colour segment derives from one particular cell. Figure 6 shows how some migrated cells give rise to a large portion of the neointima, whereas others form much smaller colonies. Also higher injury scores induce a large number of colonies: indeed, the number of colours agrees with the number of migrated SMCs.

Figure 7 qualitatively compares the rate of tissue growth in all scenarios. The simulation results suggest that a higher injury score corresponds to a slightly faster tissue growth after 14 days post-stenting. To characterize the progression of neointima formation in detail, figure 8 plots the number of neointimal cells as a function of time for all injury scenarios. The data show an increase in the number of neointimal cells as a function of time for all injury scenarios. The growth speed increases with injury score, except for the Inj_BA and Inj1 scenarios, where a complete overlap of the growth response is observed. It is worth noting here that counting of the neointimal cells also includes migrated cells, because they are also part of the neointimal tissue. It is evident from figure 8 that the rate at which SMCs proliferated increases with the injury, resulting in a faster neointimal growth with a deeper injury, although this statement does not satisfy the overlap between the Inj_BA and Inj1 groups (Inj1_20 and Inj1_40). Neointimal cells are only counted until 14 days after stenting, because there is no stopping mechanism (except contact inhibition) in the current model that can inhibit or stop cell proliferation, unless the vessel is completely occluded. In another model, where we do include such stopping mechanisms (re-endothelialization and blood flow), we find that the growth rate starts to decrease around 14 days [10,17].

Figure 8 also shows that the growth response for each injury scenario follows an exponential trend during the initial

few days after stenting and after which the growth trends become approximately linear. However, the exponential growth in the first few days is less prominent for the higher injury (Inj3). Therefore, to further elucidate the cell proliferation response in each injury scenario, exponential regression is applied to the neointimal cell count data. For such regression analyses where trends change from exponential to linear, the quality of the regressions tremendously differs depending on the fitted time interval (the time interval in which regression analysis is carried out). The parameters such as initial number of cells (N_0), the growth rate (r) and the quality of the fitting (R^2) obtained from the exponential regression analyses are shown in figure 9 and plotted as a function of the fitted time interval for each injury scenario. Figure 9 clearly shows that the quality of the fitting (R^2) goes down with an increase in the fitted time interval and this decrease in regression quality suggests that the growth trends start to deviate from exponential growth. It is also clear from the regression analysis that N_0 increases with an increase in the injury. An opposite behaviour is observed for the growth rate.

Surface tension (γ) between two cell types can have an impact on the cell migration. Therefore, in the absence of cell proliferation, a few simulations were run by varying the magnitude of surface tension between SMCs and IEL (figure 10a). It was observed that negative values of γ promote higher cell migration, whereas zero or positive values of γ inhibit complete cell migration (figure 10b).

4. Discussion

Our computational results suggest that the migrated SMCs through the IEL fenestrae play the most important role in the ISR development during the first few days and clearly show the involvement of migrated SMCs in the growth of neointima. Measuring the mean distance between the IEL cells has also elucidated the possible effects of stenting on the stretch of the IEL fenestrae (electronic supplementary material, figure S3). The results suggest that IEL holes become larger in the regions where struts were deployed, and the magnitude of such enlargement in the hole sizes directly correlates with the strut deployment depth (injury), which in turn correlates with the number of migrated SMCs and the rate of neointima formation.

The initial number of SMCs migrated into the lumen further dictates how fast a neointima will grow: a higher number of migrated cells corresponds to a faster neointimal growth as evident from figures 5, 7 and 8. According to our hypothesis, SMC migration is key in building a base for neointimal development and depending on the degree of injury, the number of migrated SMCs varies leading to different neointimal growths. Unfortunately, there are no quantitative *in vivo* data available to validate this. Apart from this, our computational proliferation growth trends (figures 7 and 8) qualitatively match well with the stented porcine coronary arteries *in vivo* data (electronic supplementary material, figure S5), in the sense that the *in vivo* data show a positive correlation between the rate of neointima formation and injury score, as in our model (figures 7 and 8). In this study, we verified our hypothesis that migration of SMCs through the fenestrae of IEL into the lumen is needed to start neointima formation and that the number of migrated SMCs correlates with the injury score. Therefore, based on the results presented in
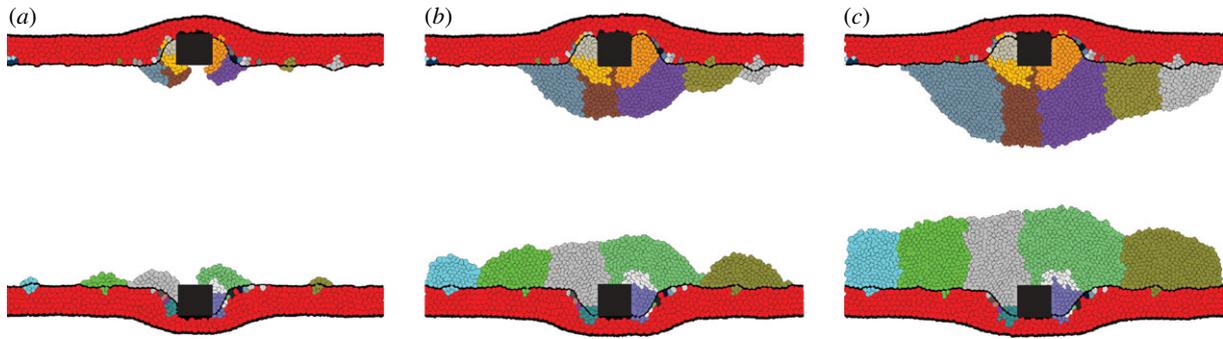
Figure 6. Progression of neointima owing to SMC proliferation at follow-up time points (*a*) at seventh day, (*b*) at 14th day and (*c*) at 21st day. The stent is deployed at 90 μm (Inj2_90). Cells with the same colour (except red) indicate that they all descended from the same mother SMC that migrated into the lumen immediately after stenting.
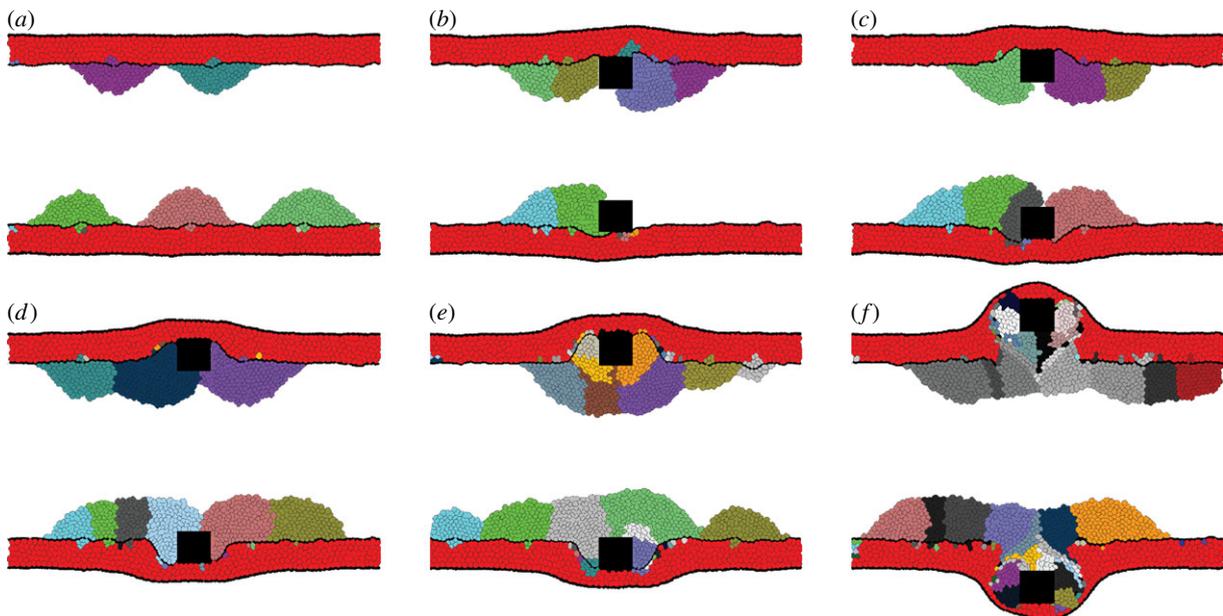

Figure 7. A qualitative comparison of neointimal tissue growth among all injury scenarios. The snapshots are taken after 14 days post-stenting. Black squares in each segment are the stent struts, whereas different colour segments of tissue in these images represent different colonies of tissue originated from individual cells. (*a*) Inj_BA, (*b*) Inj1_20, (*c*) Inj1_40, (*d*) Inj2_70, (*e*) Inj2_90 and (*f*) Inj3.
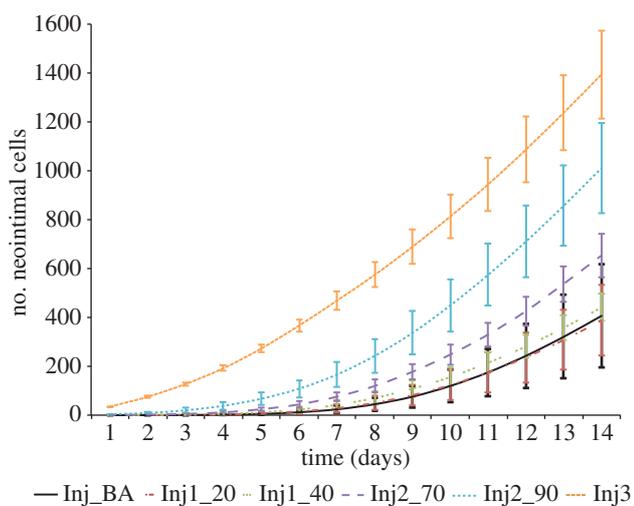

Figure 8. The growth of the neointimal tissue as a function of time for all the injury scenarios. (Online version in colour.)

this study, we postulate that the mechanism of SMC migration could explain the observed positive correlation between injury score and neointima formation.

Spatial variations and cell density have been observed to play an instructive role during cell cycle progression [41,44]. Moreover, a reduction in the available space has been observed to cause cell cycle arrest by preventing the cell from entering into the S-phase [44]. To further understand the growth dynamics of SMCs after stenting, we undertook exponential regression analysis (figure 9) on the data shown in figure 8. Although a direct relationship between the cell proliferation and the injury has been observed in figure 8, the exponential regression analysis results in an opposite reaction showing a lower growth rate associated with a higher injury. This reverse behaviour is mainly due to the reason that as more and more cells proliferate next to each other, the contact inhibition rule owing to space constraints (crowding of cells) is putting more cells back to the G0 state, resulting in a decrease in the growth rate. Cells usually follow an exponential growth but, assuming a fixed available space for the cells to grow, a faster proliferation of cells in the free regime will sooner turn the exponential growth dynamics into a linear growth regime where only the cells at the inner boundary (luminal side) of the restenosis are growing and the cells inside the tissue turn into quiescent. In the case of a deeper injury, more cells migrated into the lumen and entered into the
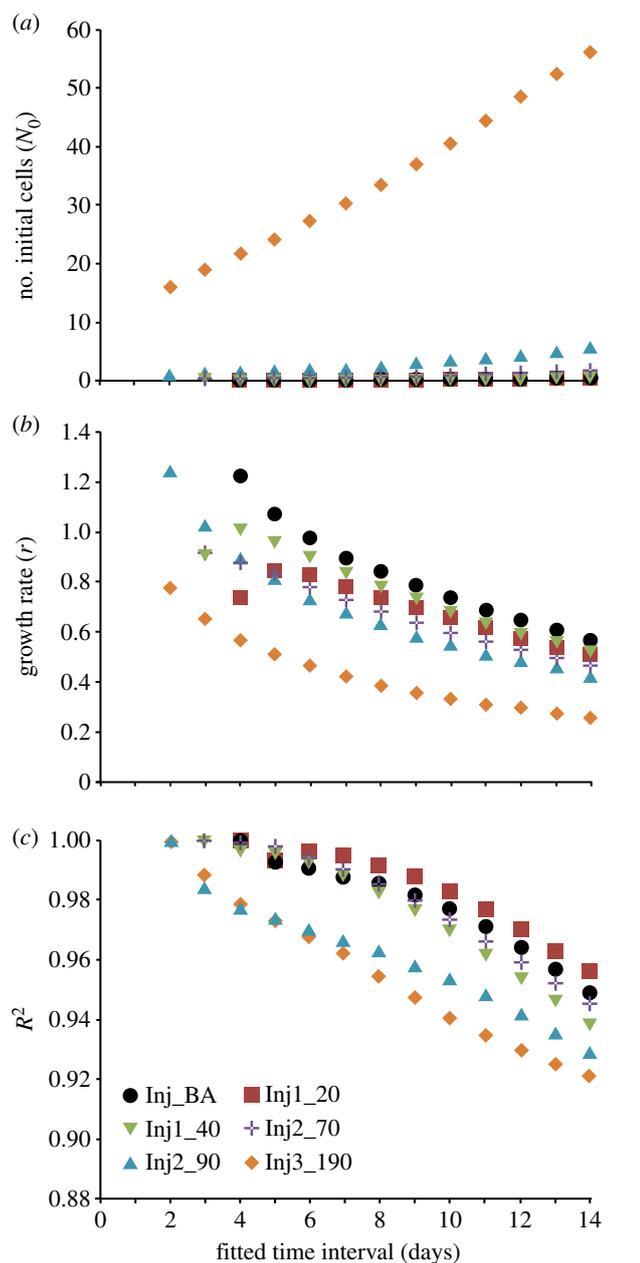
Figure 9. Exponential regression analysis on the averaged neointimal cell counts from all injury scenarios as a function of the fitted time interval. The time frame in which the data were fitted is referred to as fitted time interval, and based on this, the data are fitted using different fitted time intervals. The values of fitting parameters are retrieved from the regression analyses applied to every simulation result in each injury scenario. (a) Initial number of cells from the fitting (N_0), (b) growth rate r and (c) the quality of fitting as assessed by R-square (R^2). (Online version in colour.)

Figure 10. Surface tension (IEL–SMC) and its influence on SMC migration. Surface tension (γ) was varied in the absence of SMC proliferation to observe difference in the SMC migration. (a) Snapshots of the lower half of the stented vessel showing SMC migration through the IEL layer under different IEL–SMC surface tensions. (b) Number of migrated SMCs as a function of surface tension (IEL–SMC).

proliferative state when compared with the initial number of migrated cells at lower injuries. This increase in the cell number near the stent struts activates the contact inhibition rule a way advance when compared with lower injury scenarios, resulting in a decrease in the growth rate. The experimental observations [41,44] principally agree with the growth trends observed in this study where we start to see a decrease in the cell proliferation owing to increasing cell density (figures 8 and 9).

The emergence of the tissue clones (figures 6 and 7) derived from a few particular cells does suggest that ISR starts close to the struts. Very similar clones have been identified in bacterial colonies where they were attributed to spatial competition [45],
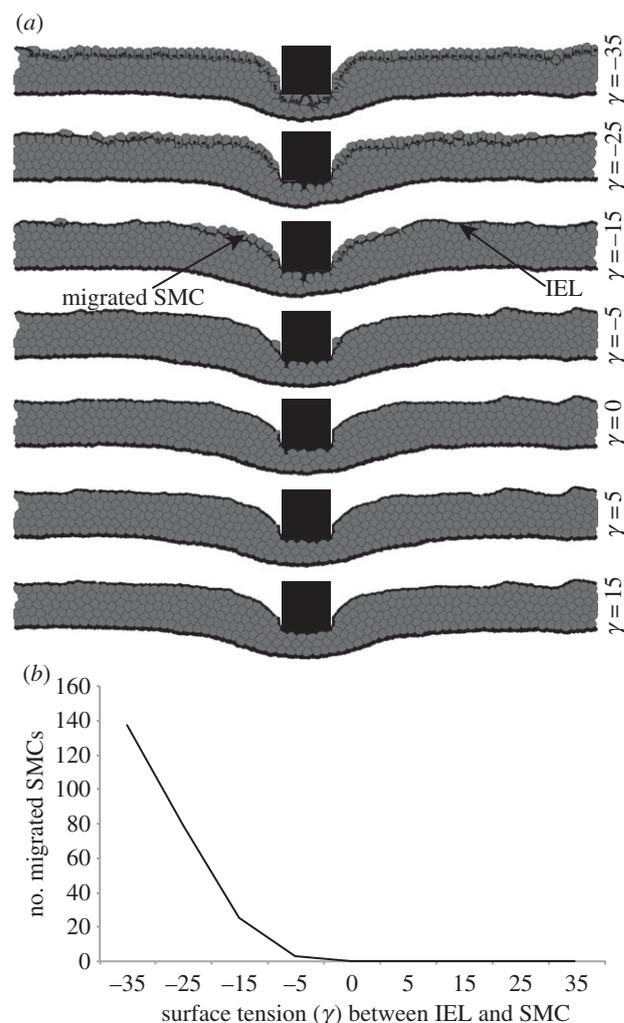
but according to the best of our knowledge, there is no available evidence for the predicted clonar pattern in vascular tissue histology or animal experiments. Detailed histological studies, e.g. using fluorescent labelling or DNA barcoding techniques, should confirm if such kind of tissue segments do appear in reality or not. Moreover, we also observe very little initial proliferation of the synthetic cells inside the medial wall, which stopped after some time as those cells were not able to cross the IEL layer and became quiescent again owing to contact inhibition. The observation may further convince clinicians in this field to investigate the evolution of cellular growth by tracking the migration and growth from individual cells in real animal arteries and such data will also be required to validate our tissue model.

In this study, we observed single cell motility of the SMCs rather than observed a collective cell migration. Strong cell–cell junctions are necessary for collective cell migration [12]. However, after SMC phenotypic modulation from contractile to synthetic, SMCs lose adherent junctions and become less adhesive to neighbouring cells [13,34], thus suggesting the presence of single cell migration as we observe in this study. This however warrants the need for further detailed *in vivo* experiments by tracking individual cells. SMCs are multifunctional

cells, and cell contractility is a central property of the SMCs under physiological conditions. Under pathological conditions, these cells undergo phenotypic modulation and lose their contractile properties and become highly plastic [46–48]. Because we are mainly studying the role of SMC migration and proliferation under pathological conditions, we have neglected the role of SMC contractility in this study. The current ISR model has been used as a stand-alone model where no interaction with the blood flow has been taken into account. This existing CPM can further be coupled with a flow model to observe the influence of blood flow on the dynamics of SMC migration and proliferation. This will be considered as a next step forward in developing coupled CPM–flow models.

To conclude, an *in silico* CPM of a two-dimensional stented vessel has been developed that allows us to investigate the role of SMC migration during ISR development. This study has allowed us to test and prove our hypothesis that the development of neointimal tissue heavily depends on the number of initial migrated SMCs within the first few hours or days. A decrease or increase in the number of migrated SMCs during the early days seems to have a dominant effect on the speed of neointimal growth. This hypothesis however warrants some further detailed animal experiments, focused on capturing the initial tissue response at a cellular scale and this still might be far from trivial owing to the complexity and limited availability of imaging techniques to specifically visualize and track single cells within a live arterial vessel. From our experience in modelling ISR (CPM-based ISR model and our other coupled ISR models) [10,16,17], we however suggest a complete set of hypotheses that initial migration of the SMCs in response to injury determines how fast the tissue will grow, whereas the regeneration of the endothelium and EC ability to regain their functionality determines if a patient is going to develop ISR or not. Any alterations in the above would determine how fast and how much neointima a patient is going to develop.

References

1. Otsuka F, Finn AV, Yazdani SK, Nakano M, Kolodgie FD, Virmani R. 2012 The importance of the endothelium in atherothrombosis and coronary stenting. *Nat. Rev. Cardiol.* **9**, 439–453. (doi:10.1038/nrcardio.2012.64)

2. Harnek J, Zoucas E, Carlemalm E, Cwikiel W. 1999 Differences in endothelial injury after balloon angioplasty, insertion of balloon-expanded stents or release of self-expanding stents: an electron microscopic experimental study. *Cardiovasc. Intervent. Radiol.* **22**, 56–61. (doi:10.1007/s002709900329)

3. Gunn J, Arnold N, Chan KH, Shepherd L, Cumberland DC, Crossman DC. 2002 Coronary artery stretch versus deep injury in the development of in-stent neointima. *Heart* **88**, 401–405. (doi:10.1136/heart.88.4.401)

4. Jukema JW, Verschuren JJW, Ahmed TAN, Quax PHA. 2011 Restenosis after PCI. Part 1: pathophysiology and risk factors. *Nat. Rev. Cardiol.* **9**, 53–62. (doi:10.1038/nrcardio.2011.132)

5. Marx SO, Totary-Jain H, Marks AR. 2011 Vascular smooth muscle cell proliferation in restenosis. *Circulation* **4**, 104–111. (doi:10.1161/CIRCINTERVENTIONS.110.957332)

6. Levitzki A. 2005 PDGF receptor kinase inhibitors for the treatment of restenosis. *Cardiovasc. Res.* **65**, 581–586. (doi:10.1016/j.cardiores.2004.08.008)

7. Kirby BS, Bruhl A, Sullivan MN, Francis M, Dinenno FA, Earley S. 2013 Robust internal elastic lamina fenestration in skeletal muscle arteries. *PLoS ONE* **8**, e54849. (doi:10.1371/journal.pone.0054849)

8. Sandow SL, Gzik DJ, Lee RM. 2009 Arterial internal elastic lamina holes: relationship to function? *J. Anat.* **214**, 258–266. (doi:10.1111/j.1469-7580.2008.01020.x)

9. Thyberg J, Blomgren K, Hedin U, Dryjski M. 1995 Phenotypic modulation of smooth muscle cells during the formation of neointimal thickenings in the rat carotid artery after balloon injury: an electron-microscopic and stereological study. *Cell Tissue Res.* **281**, 421–433. (doi:10.1007/BF00417860)

10. Tahir H, Hoekstra AG, Lorenz E, Lawford PV, Hose DR, Gunn J, Evans DJW. 2011 Multi-scale simulations of the dynamics of in-stent restenosis: impact of stent deployment and design. *Interface Focus* **1**, 365–373. (doi:10.1098/rsfs.2010.0024)

11. Welt FGP, Rogers C. 2002 Inflammation and restenosis in the stent era. *Arterioscler. Thromb. Vasc. Biol.* **22**, 1769–1776. (doi:10.1161/01.ATV.0000037100.44766.5B)

12. Louis SF, Zahradka P. 2010 Vascular smooth muscle cell motility: from migration to invasion. *Exp. Clin. Cardiol.* **15**, e75–e85.

13. Fukui R *et al.* 2000 Increased migration in late G1 phase in cultured smooth muscle cells. *Am. J. Physiol. Cell Physiol.* **279**, C999–C1007.

14. Poon M, Marx SO, Gallo R, Badimon JJ, Taubman MB, Marks AR. 1996 Rapamycin inhibits vascular smooth muscle cell migration. *J. Clin. Invest.* **98**, 2277–2283. (doi:10.1172/JCI119038)

15. Sollott SJ *et al.* 1995 Taxol inhibits neointimal smooth muscle cell accumulation after angioplasty in the rat. *J. Clin. Invest.* **95**, 1869–1876. (doi:10.1172/JCI117867)

16. Tahir H, Bona-Casas C, Narracott AJ, Iqbal J, Gunn J, Lawford P, Hoekstra AG. 2014 Endothelial repair process and its relevance to longitudinal neointimal tissue patterns: comparing histology with *in silico* modelling. *J. R. Soc. Interface* **11**, 20140022. (doi:10.1098/rsif.2014.0022)

17. Tahir H, Bona-Casas C, Hoekstra AG. 2013 Modelling the effect of a functional endothelium on the development of in-stent restenosis. *PLoS ONE* **8**, e66138. (doi:10.1371/journal.pone.0066138)

18. Zahedmanesh H, Lally C. 2009 Determination of the influence of stent strut thickness using the finite element method: implications for vascular injury and in-stent restenosis. *Med. Biol. Eng. Comput.* **47**, 385–393. (doi:10.1007/s11517-009-0432-5)

19. Keller BK *et al.* 2014 Contribution of mechanical and fluid stresses to the magnitude of in-stent restenosis at the level of individual stent struts. *Cardiovasc. Eng. Technol.* **5**, 164–175. (doi:10.1007/s13239-014-0181-y)

20. Swat MH, Thomas GL, Belmonte JM, Shirinifard A, Hmeljak D, Glazier JA. 2012 Multi-scale modeling of tissues using CompuCell3D. *Methods Cell. Biol.* **110**, 325–366. (doi:10.1016/B978-0-12-388403-9.00013-8)

21. van Oers RFM, Rens EG, LaValley DJ, Reinhart-King CA, Merks RMH. 2014 Mechanical cell-matrix feedback explains pairwise and collective endothelial cell behavior *in vitro*. *PLoS Comput. Biol.* **10**, e1003774. (doi:10.1371/journal.pcbi.1003774)

22. Chiu J-J, Chien S. 2011 Effects of disturbed flow on vascular endothelium: pathophysiological basis and clinical perspectives. *Physiol. Rev.* **91**, 327–387. (doi:10.1152/physrev.00047.2009)

23. Redmond EM, Lally C, Cahill PA. 2012 Hemodynamic control of vascular smooth muscle function. In *Muscle: fundamental biology and mechanisms of disease*, vol. 2 (eds JA Hill, EN Olson), pp. 1231–1242. Amsterdam, The Netherlands: Elsevier. (doi:10.1016/b978-0-12-381510-1.00092-2)

24. de Prado AP *et al.* 2011 Time course of reendothelialization of stents in a normal coronary swine model. *Vet. Pathol. Online* **48**, 1109–1117. (doi:10.1177/0300985811400446)

25. Glazier JA, Graner F. 1993 Simulation of the differential adhesion driven rearrangement of biological cells. *Phys. Rev. E* **47**, 2128–2154. (doi:10.1103/PhysRevE.47.2128)

26. Graner F, Glazier JA. 1992 Simulation of biological cell sorting using a two-dimensional extended Potts model. *Phys. Rev. Lett.* **69**, 2013–2016. (doi:10.1103/PhysRevLett.69.2013)

27. Nakajima A, Ishihara S. 2011 Kinetics of the cellular Potts model revisited. *N. J. Phys.* **13**, 033035. (doi:10.1088/1367-2630/13/3/033035)

28. Merks RMH. 2006 Tissue simulation toolkit. http://sourceforge.net/projects/tst.

29. Merks RMH, Glazier JA. 2005 A cell-centered approach to developmental biology. *Physica A* **352**, 113–130. (doi:10.1016/j.physa.2004.12.028)

30. Daub JT, Merks RMH. 2015 Cell-based computational modeling of vascular morphogenesis using tissue simulation toolkit. In *Vascular morphogenesis* (ed. D Ribatti), pp. 67–127. New York, NY: Springer. (doi:10.1007/978-1-4939-1462-3_6)

31. DiMilla PA, Stone JA, Quinn JA, Albelda SM, Lauffenburger DA. 1993 Maximal migration of human smooth muscle cells on fibronectin and type IV collagen occurs at an intermediate attachment strength. *J. Cell Biol.* **122**, 729–737. (doi:10.1083/jcb.122.3.729)

32. Majesky MW. 1994 Neointima formation after acute vascular injury. Role of counteradhesive extracellular matrix proteins. *Texas Heart Inst. J.* **21**, 78.

33. Moiseeva EP. 2001 Adhesion receptors of vascular smooth muscle cells and their functions. *Cardiovasc. Res.* **52**, 372–86. (doi:10.1016/S0008-6363(01)00399-6)

34. Rensen SSM, Doevendans PAFM, Van Eys GJJM. 2007 Regulation and characteristics of vascular smooth muscle cell phenotypic diversity. *Netherlands Heart J.* **15**, 100–108. (doi:10.1007/BF03085963)

35. Niculescu I. 2011 Towards a cell-based model of neointimal hyperplasia with cellular Potts model. MSc thesis, University of Amsterdam. http://www.science.uva.nl/research/scs/papers/archive/Niculescu2011a.pdf.

36. Kwon HM, Sangiorgi G, Spagnoli LG, Miyauchi K, Holmes Jr DR, Schwartz RS, Lerman A. 1998 Experimental hypercholesterolemia induces ultrastructural changes in the internal elastic lamina of porcine coronary arteries. *Atherosclerosis* **139**, 283–289. (doi:10.1016/S0021-9150(98)00081-1)

37. Aiello VD, Gutierrez PS, Chaves MJF, Lopes AAB, Higuchi ML, Ramires JAF. 2003 Morphology of the internal elastic lamina in arteries from pulmonary hypertensive patients: a confocal laser microscopy study. *Mod. Pathol.* **16**, 411–416. (doi:10.1097/01.MP.0000067685.57858.D7)

38. Breton M, Berrou E, Brahimi-Horn M, Deudon E, Picard J. 1986 Synthesis of sulfated proteoglycans throughout the cell cycle in smooth muscle cells from pig aorta. *Exp. Cell Res.* **166**, 416–426. (doi:10.1016/0014-4827(86)90487-8)

39. Walker DC, Hill G, Wood SM, Smallwood RH, Southgate J. 2004 Agent-based computational modeling of wounded epithelial cell monolayers. *IEEE Trans. Nanobiosci.* **3**, 153–163. (doi:10.1109/TNB.2004.833680)

40. Walker DC, Southgate J, Hill G, Holcombe M, Hose DR, Wood SM, Neil SM, Smallwood RH. 2004 The epitheliome: agent-based modelling of the social behaviour of cells. *Biosystems* **76**, 89–100. (doi:10.1016/j.biosystems.2004.05.025)

41. Puliafito A, Hufnagel L, Neveu P, Streichan S, Sigal A, Fygenson DK, Shraiman BI. 2012 Collective and single cell behavior in epithelial contact inhibition. *Proc. Natl Acad. Sci. USA* **109**, 739–744. (doi:10.1073/pnas.1007809109)

42. Caiazzo A *et al.* 2011 A complex automata approach for in-stent restenosis: two-dimensional multiscale modelling and simulations. *J. Comput. Sci.* **2**, 9–17. (doi:10.1016/j.jocs.2010.09.002)

43. Landau C, Lange RA, Hillis LD. 1994 Percutaneous transluminal coronary angioplasty. *N. Engl. J. Med.* **330**, 981–993. (doi:10.1056/NEJM199404073301407)

44. Streichan SJ, Hoerner CR, Schneidt T, Holzer D, Hufnagel L. 2014 Spatial constraints control cell proliferation in tissues. *Proc. Natl Acad. Sci. USA* **111**, 5586–5591. (doi:10.1073/pnas.1323016111)

45. Xavier JB. 2011 Social interaction in synthetic and natural microbial communities. *Mol. Syst. Biol.* **7**, 483. (doi:10.1038/msb2011.16)

46. Chamley-Campbell J, Campbell GR, Ross R. 1979 The smooth muscle cell in culture. *Physiol. Rev.* **59**, 1–61.

47. Nguyen AT *et al.* 2013 Smooth muscle cell plasticity fact or fiction? *Circ. Res.* **112**, 17–22. (doi:10.1161/CIRCRESAHA.112.281048)

48. Mitra A, Agrawal D. 2006 In stent restenosis: bane of the stent era. *J. Clin. Pathol.* **59**, 232–239. (doi:10.1136/jcp.2005.025742)